Tunable Photoluminescent and Cathodoluminescent Properties of ZnO and ZnO:Zn Phosphors

Zhenling Wang, Cuikun Lin, Xiaoming Liu, Guangzhi Li, Yan Luo, Zewei Quan, Hongping Xiang, and Jun Lin*

Key Laboratory of Rare Earth Chemistry and Physics, Changchun Institute of Applied Chemistry, Chinese Academy of Sciences, Changchun 130022, and Graduate School of the Chinese Academy of Sciences, Beijing 100049, P R China

Received: December 10, 2005; In Final Form: March 22, 2006

ZnO and ZnO:Zn powder phosphors were prepared by the polyol-method followed by annealing in air and reducing gas, respectively. The samples were characterized by X-ray diffraction (XRD), field emission scanning electron microscopy (FESEM), X-ray photoelectron spectra (XPS), electron paramagnetic resonance (EPR), and photoluminescence (PL) and cathodoluminescence (CL) spectra, respectively. The results indicate that all samples are in agreement with the hexagonal structure of the ZnO phase and the particle sizes are in the range of 1−2 μm. The PL and CL spectra of ZnO powders annealed at 950 °C in air consist of a weak ultraviolet emission band (∼390 nm) and a broad emission band centered at about 527 nm, exhibiting yellow emission color to the naked eyes. When the sample was reduced at the temperatures from 500 to 1050 °C, the yellow emission decreased gradually and disappeared completely at 800 °C, whereas the ultraviolet emission band became the strongest. Above this temperature, the green emission (∼500 nm) appeared and increased with increasing of reducing temperatures. According to the EPR results and spectral analysis, the yellow and green emissions may arise from the transitions of photogenerated electron close to the conduction band to the deeply trapped hole in the single negatively charged interstitial oxygen ion (O_i^-) and the single ionized oxygen vacancy ($V_O^\bullet$) centers, respectively.

1. Introduction

There are a large number of technologies used for flat panel displays (FPDs), including emissive and nonemissive ones.[1] Among the emissive display technologies, field emission displays (FEDs) have been developed as a future promising emissive display realizing high resolution and low consumption of electric power.[2] Phosphors used in FEDs require several new properties that the traditional cathode ray tube (CRT) phosphors may not possess, such as high electric conductivity, low surface recombination velocities, vacuum compatibility (low outgassing), hazardless to cathodes, and the ability to withstand high current densities.[3] For example, the most popular sulfide-based phosphors for CRTs are no longer suitable for FEDs because of the low conductivity and the fast degradation at high current densities.[4] Therefore, the development of oxide-based phosphors has become a necessity. As a wide band gap semiconductor, zinc oxide (ZnO) has been known as a luminescent material for a long time, and it is of great interest for photonic applications such as UV luminescent devices, low threshold lasers, nonlinear optical devices and so forth.[5] ZnO is a self-activated phosphor that has good characteristics such as low outgassing, high electric conductivity (∼10^{-3} $\Omega\cdot cm^{-1}$), low excitation voltage, and high stability.[6] The reduced form of ZnO, usually denoted as ZnO:Zn, exhibits bright green luminescence and has been proved to be a good candidate for FEDs phosphor with low-voltage excitation.[3b,4b,7] ZnO:Zn powder phosphors have been prepared by solid-state sintering of mixtures of ZnO and ZnS powders in a N_2 atmosphere.[8] Because the particle size is critical to loading on screens and improving the resolution of a display,[1a] the ZnO:Zn samples obtained by this method are often powders with a few micrometers, which are obviously too rough to be used in FEDs where the anode−cathode distance is only 10−200 μm.[9] To overcome this disadvantage, ZnO:Zn phosphor thin films have been prepared by ion beam sputtering, rf-magnetron sputtering, filtered arc deposition, and other physical methods.[3b,7a,10a,b] The ZnO:Zn phosphor thin films prepared by these physical methods may have the characteristics of smooth, conductive, and well substrate-combined, however, the key problem is that the luminescent intensity is not strong enough compared with the powder phosphors. In addition, the demand of the preparation conditions for physical methods is not easy to realize. So it is necessary to explore a simple procedure to synthesize the ZnO:Zn phosphors with the unique particle size. The monodisperse ZnO particles with size from 100 to 600 nm can be obtained by a two-stage chemical reaction process.[10c] However, the photoluminescence or cathodoluminescence intensities of the as-prepared ZnO particles are very weak. To improve the luminescence intensity, heat treatment for the as-prepared ZnO particles is necessary. We hope that the luminescent properties of ZnO particles can be enhanced to a great degree without destroying the good morphology of the as-prepared samples after annealing at high temperature.

Generally, ZnO can show three luminescence bands in the ultraviolet (UV), green, and yellow regions. The UV emission has been well understood, which arises from the direct recombination of photogenerated charge carriers (exciton emission).[11] However, there are various mechanisms responsible for visible emission, such as the involvement of O vacancies,[3a,b,11a,12]

* Corresponding author. Tel: +86-431-5262031. Fax: +86-431-5698041. E-mail: jlin@ciac.jl.cn.

10.1021/jp057214t CCC: $33.50
Published on Web 04/21/2006

interstitial O,[11a,13] Zn vacancies, Zn interstitials,[7b] oxide antisite defect (O_{Zn}),[14] surface defects,[15] and so forth. It is important to understand the luminescence mechanism for adjusting luminescent properties and improving the luminescent efficiency. In this paper, ZnO and ZnO:Zn powders were prepared by the polyol-method followed by annealing in air and reducing gas, respectively. The ultraviolet, yellow, and green emissions of ZnO powders can be adjusted easily by annealing conditions. The luminescence mechanisms responsible for the yellow and green emissions were also discussed.

2. Experimental Section

Spherical ZnO particles were prepared by the polyol-method as described previously.[10c] Typically, 0.03 mol zinc acetate dihydrate ($Zn(CH_3CO_2)_2 \cdot 2H_2O$, 99.0%, analytical reagent, A. R., Shanghai Jinshan Chemical Reagent Corporation) was added to 300 mL diethylene glycol (DEG, 98%, A. R., Beijing Yili Chemical Reagent Corporation). This reaction solution was heated to 160 °C and held for 1h, then cooled to room temperature with precipitation occurred. The precipitates were separated by centrifugation, washed with ethanol, and dried at 100 °C. The as-prepared ZnO particles were annealed at different temperatures in air for 2h with a heating rate of 5 °C·min^{-1}. The resulted ZnO powders are denoted as "ZnO-temperature". ZnO:Zn powders were obtained by sintering parts of the ZnO-temperature samples in a flow of reducing gas (95% N_2 + 5% H_2 in volume, 99.999% pure) at different temperatures for a desired time with a heating rate of 10 °C·min^{-1}.

X-ray diffraction (XRD) was carried out on a Rigaku-Dmax 2500 diffractometer with Cu Kα radiation ($\lambda = 0.15405$ nm) (40 kV, 200 mA). SEM micrographs were obtained using a field emission scanning electron microscope (FE-SEM, XL30, Philips). The X-ray photoelectron spectra (XPS) were taken on a VG ESCALAB MK II electron spectrometer using Mg Kα (1253.6 eV) as the exciting source. Electron paramagnetic resonance (EPR) measurements were performed using an X-band (9.440 GHz) JES-FE3AX spectrometer (JEOL) at 293 K. Cylindrical quartz-tube containers were used to insert the powders into the microwave cavity. The atomic absorption spectra (AAS, P-E Analyst 800) and energy disperse spectra (EDS, ISIS-300, attached to JXA-840 Scanning Microanalyzer, accelerating voltage: 20 kV) were used to measure the Zn/O ratios of the prepared samples. The photoluminescence (PL) spectra were taken on an F-4500 spectrophotometer equipped with a 150 W xenon lamp as the excitation source, and the excitation wavelength was kept at 350 nm. The cathodoluminescent (CL) spectra were measured with a self-made CL system with an accelerating voltage in the range of 0.8−4.0 kV.

3. Results and Discussion

Phase Structure and Morphology. To investigate the effect of reducing treatment on the phase structure of ZnO powders, we reduced portions of ZnO powders annealed at 600, 800, and 1050 °C at the corresponding temperature for 30 min. Figure 1 shows the XRD patterns of the as-prepared ZnO (b), ZnO-600 °C (c), ZnO:Zn-600 °C (d), ZnO-800 °C (e), ZnO:Zn-800 °C (f), ZnO-1050 °C (g), and ZnO:Zn-1050 °C (h) powders and the standard data (a) for ZnO bulk powders. The results of XRD indicate that the as-prepared samples are well crystallized and the diffraction peaks are in good agreement with hexagonal structure of ZnO phase (JCPDS Card no. 36-1451). With the increase of annealing temperatures, the peak intensities increase and the width of these peaks become sharper because of the improvement of crystallization. No apparent difference in the XRD patterns is observed for ZnO and ZnO:Zn powders annealed at the same temperature. The reducing gas annealing is thought to etch the surface of the ZnO particles. Zn atoms are released in this process, so the reducing treatment is physically similar to the annealing of ZnO powders in a Zn-rich ambient.[3a] The Zn atoms may diffuse to the interstitial sites, the host lattices, or the oxygen vacancies created in ZnO lattices during the reducing treatment.[8b] So the patterns of metal Zn are not present in Figure 1 for the ZnO:Zn samples. Table 1 shows the lattice parameters and the corresponding standard deviations (compared with the data of the JCPDS Card) of the same samples in Figure 1 calculated on the basis of XRD data. Because of the different preparation procedures, the calculated crystal cell parameters for all samples are slightly different from the data of the JCPDS Card ($a = b = 0.325$ nm, $c = 0.5207$ nm). Both lattice parameters a and c of ZnO:Zn powders are a little smaller than those of the corresponding ZnO powders. This suggests that parts of Zn atoms may diffuse to occupy the oxygen vacancies because the presence of Zn in the interstitial site would enhance the lattice parameters.[8b]

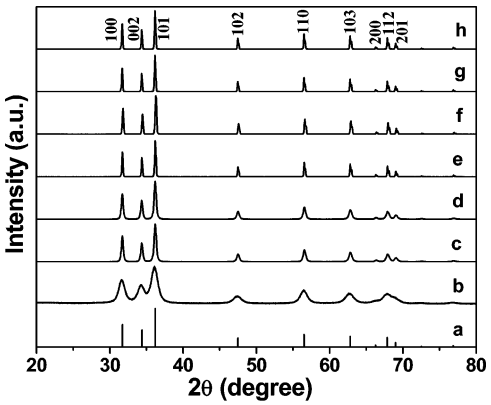

Figure 1. XRD patterns of the as-prepared ZnO (b), ZnO-600 °C (c), ZnO:Zn-600 °C (d), ZnO-800 °C (e), ZnO:Zn-800 °C (f), ZnO-1050 °C (g), and ZnO:Zn-1050 °C (h) powders and the standard data for ZnO (a, JCPDS Card no. 36-1451).

TABLE 1: Crystal Cell Parameters of As-Prepared ZnO, ZnO-600 °C, ZnO-800 °C, ZnO-1050 °C, ZnO:Zn-600 °C, ZnO:Zn-800 °C, and ZnO:Zn-1050 °C Powders, Calculated on the Basis of XRD Data Shown in Figure 1[a]

	ZnO	ZnO -600 °C	ZnO:Zn -600 °C	ZnO -800 °C	ZnO:Zn -800 °C	ZnO -1050 °C	ZnO:Zn -1050 °C
a (nm)	0.3257	0.3255	0.3255	0.3255	0.3250	0.3259	0.3252
σ_a	0.0022	0.0015	0.0015	0.0015	0.0000	0.0028	0.0006
c (nm)	0.5233	0.5216	0.5216	0.5213	0.5198	0.5216	0.5208
σ_c	0.0050	0.0017	0.0017	0.0012	−0.0017	0.0017	0.0002

[a] The data of σ_a and σ_c are the corresponding standard deviations of a and c parameters, respectively.

The morphologies of as-prepared ZnO samples and the representative ZnO and ZnO:Zn crystalline powders were observed by FESEM. Figure 2 shows the FESEM images of as-prepared ZnO (a), ZnO-950 °C (b), and ZnO:Zn-1050 °C (c) powders, respectively. It can be seen clearly that the as-prepared ZnO powders are composed of spherical particles. The average size of these particles is about 1.2 μm. After annealing at 950 °C in air for 2h, the spherical shape of ZnO particles are basically retained, whereas the ZnO particles are agglomerated slightly and their surface becomes smoother than that without annealing. After being reduced at 1050 °C for 30 min, the ZnO-950 °C powders turned to have irregular shapes with particles size increasing to 1.5−2.0 μm.

XPS, AAS, and EDS Analysis. To confirm the existence of metal Zn in the ZnO:Zn powders, ZnO-950 °C samples before

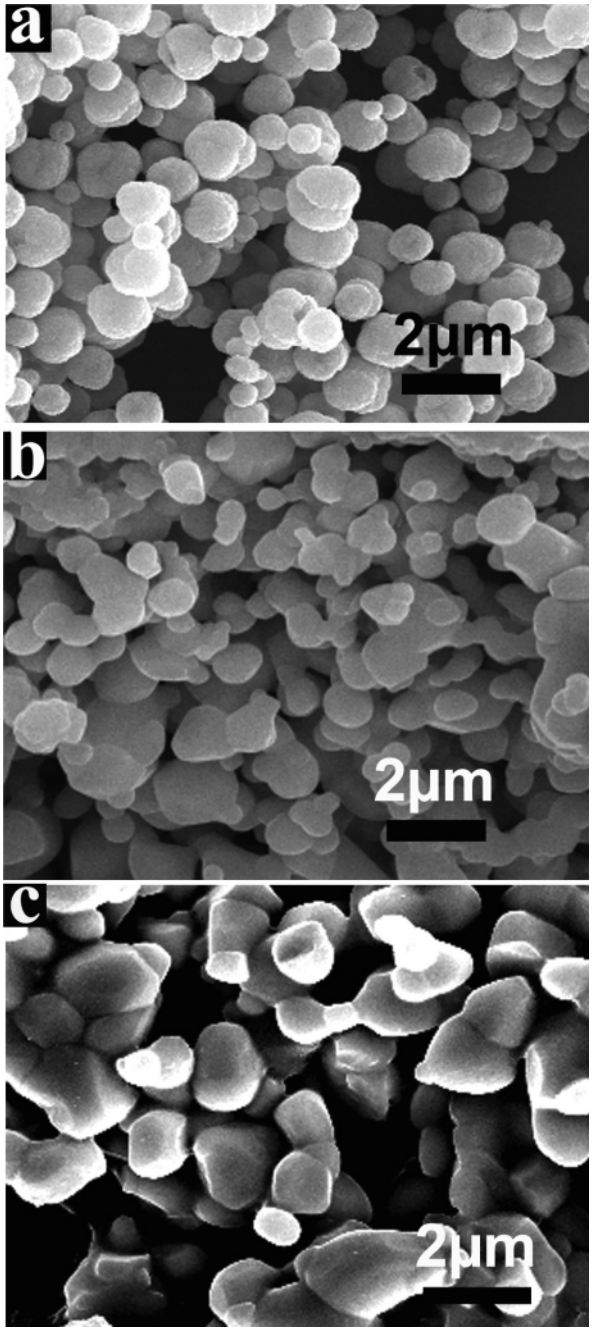

Figure 2. FE-SEM images of as-prepared ZnO (a), ZnO-950 °C (b), and ZnO:Zn-1050 °C (c) powders.

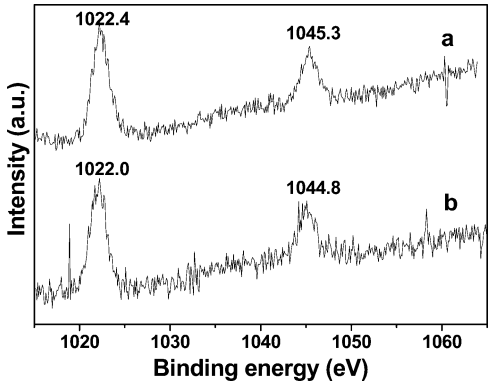

Figure 3. XPS of ZnO-950 °C (a) and ZnO:Zn-1050 °C (b) powders.

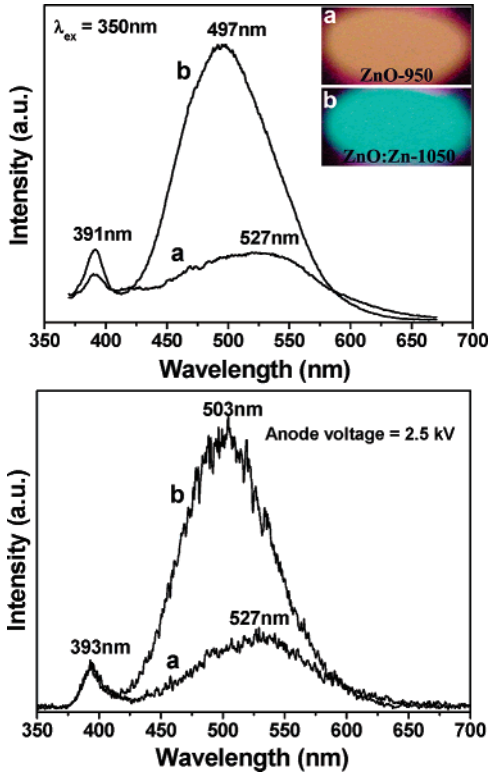

Figure 4. PL (up) and CL (bottom) spectra of ZnO-950 °C (a) and ZnO:Zn-1050 °C (b) powders. The inset is the photographs of these two powders under irradiation of a 365 nm UV lamp.

and after being reduced at 1050 °C were subjected to XPS analysis. Figure 3 shows the XPS results of ZnO-950 °C (a) and ZnO:Zn-1050 °C (b) powders, respectively. In Figure 3a, the Zn $2p_{3/2}$ and Zn $2p_{1/2}$ peaks of ZnO are located at 1022.4 and 1045.3 eV, respectively. Compared with the Zn $2p_{3/2}$ and Zn $2p_{1/2}$ binding energies of the ZnO powders, the Zn $2p_{3/2}$ and Zn $2p_{1/2}$ peaks of the ZnO:Zn powders shift to 1022.0 and 1044.8 eV, respectively, as shown in Figure 3b. The shift of these two peaks to a lower binding energy is indicative of the appearance of metal Zn in the ZnO:Zn phosphors.[16]

To build a quantitative correlation between the stoichiometry of Zn and oxygen and the reducing conditions, we tried to measure the molar ratios of Zn to O atom ($R_{Zn/O}$) by atomic absorption spectra and energy disperse spectra, and the data are collected in Table S1 (Supporting Information). Although the data are not very accurate (much higher than the actual values), they clearly reveal that the molar ratios $R_{Zn/O}$ increase with the increase of reducing temperature as we expected, that is, more metal Zn or oxygen vacancies have been produced after annealing at higher temperature.

Luminescent Properties. *PL and CL Spectra.* PL spectra are convenient tools that are used widely to evaluate the luminescent properties of ZnO based phosphors; however, it should be noted that CL spectra would be more accurate to evaluate ZnO:Zn phosphors because they can simulate the working environment of phosphors. So the PL and CL spectra of ZnO and ZnO:Zn powders were compared and discussed together. Figure 4 shows the PL (up) and CL (bottom) spectra of ZnO-950 °C (a) and ZnO:Zn-1050 °C (b) powders (the inset is the photographs of these two powders under irradiation of a 365 nm UV lamp). In Figure 4 (up), under the excitation of 350 nm UV, the PL spectra of ZnO and ZnO:Zn powders possess an ultraviolet emission band and a broad visible emission band. The ultraviolet emission bands of ZnO (a) and ZnO:Zn (b) powders are similar in profile peaking at ~391 nm, which

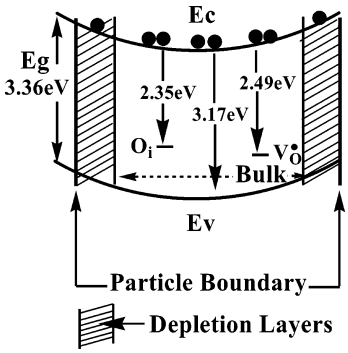

Figure 5. Schematic diagram of the energy band of a ZnO-based particle in cross section. The conduction band (Ec), valence band (Ev), band gap (Eg), single negatively charged interstitial oxygen ion (O_i^-) and single ionized oxygen vacancy ($V_O^{\bullet}$).

is attributed to the direct recombination of photogenerated charge carriers (excition emission).[11b,c,d] However, the location and intensity of visible emission bands for these two samples are different, which can be attributed to the different luminescence mechanisms. The ZnO powders have a broad emission band centered at ~527 nm, exhibiting yellow emission color to the naked eye under irradiation of a 365 nm UV lamp (Figure 4 up, a and inset), which arises from the radiative recombination of photogenerated electron close to the conduction with a deeply trapped hole in the single negatively charged interstitial oxygen ion (O_i^-) centers in the particles.[11a] For ZnO:Zn powders, there exists a strong and broad green emission band peaking at ~500 nm, exhibiting green emission color to the naked eye under irradiation of a 365 nm UV lamp, as shown in Figure 4 (up, b and inset). This green emission is attributed to the transition of a photogenerated electron close to the conduction band to a deeply trapped hole in the single ionized oxygen vacancy ($V_O^{\bullet}$).[3b,11a] The CL spectra of ZnO-950 °C and ZnO:Zn-1050 °C powders are similar to their PL spectra in profile, as shown in Figure 4 (bottom). The visible emission bands with the peaks at ~527 and ~500 nm are also attributed to the optical transitions of photogenerated electron close to the conductionin band to the single negatively charged interstitial oxygen ion (O_i^-) and the single ionized oxygen vacancy ($V_O^{\bullet}$) centers inside the grains, respectively. The schematic diagram of the radiative transitions responsible for the UV, green, and yellow emissions is shown in Figure 5.[11a]

The band structures of defective ZnO powders were calculated using CASTEP code based on the density-function theory (DFT), and exchange and correlation have been treated by the generalized gradient approximation (GGA) within the scheme due to Perdew−Burke−Ernzerhof (PBE).[17a,b] This method has been applied to many materials, such as $SrAl_2O_4:Eu^{2+}$ nanocrystals, aluminum hydroxide, and so forth.[17c−j] In this calculation, the structure models of ideal and defective ZnO, that is, oxygen vacancy (V_O) and interstitial oxygen (O_i) were established according to the literature,[17k] as shown in Figure 6 a, b, and c, respectively. The experimental data of the cell parameters listed in Table 1 were used and the atom positions were obtained from ref 17(l). The Kohn−Sham wave functions of valence electrons were expanded to the basis set of plane waves within a specified cutoff energy (E_{cut} = 340 eV). Valence electrons (O $2s^22p^4$, Zn $3d^{10}4s^2$) were described by Vanderbit-type nonlocal ultrasoft pseudopotentials.[17m] The Brillouin zone was sampled by a 4 × 4 × 2 Monkhorst-Pack mesh of K-points. The calculating parameters and convergent criteria were set by the default values of CASTEP code. The calculated band

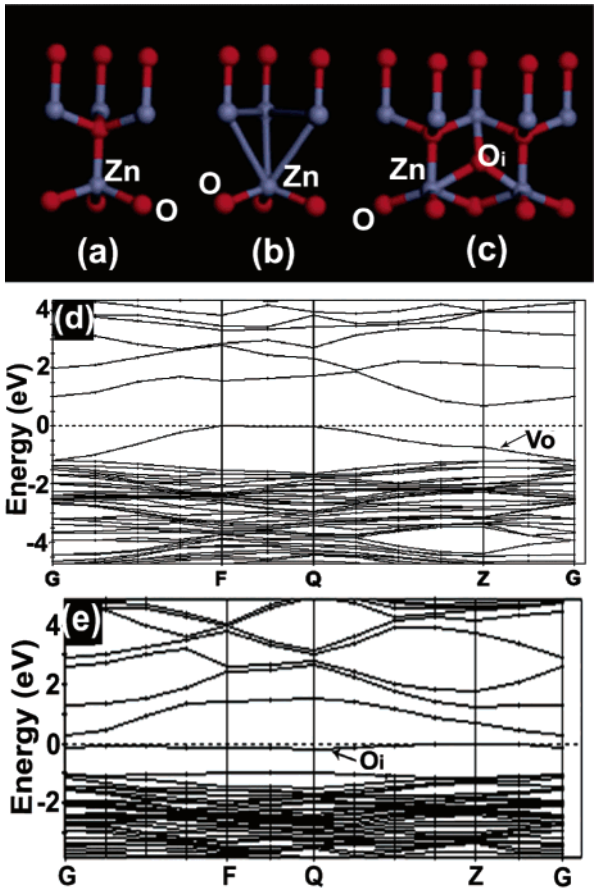

Figure 6. Structure models of ZnO: ideal (a), oxygen vacancy (b), interstitial oxygen (c), and the calculated band structures according to the model of oxygen vacancy (d) and interstitial oxygen (e). The level location of V_O center is lower than that of O_i center at G, *Z* axis (dotted line: Fermi level).

structures of defective ZnO are given in Figure 6d (V_O) and e (O_i), respectively. The calculated band gap for defective ZnO (V_O) is a little larger than that of defective ZnO (O_i), confirming the trend of the band gap relationships of the two models proposed in the luminescent mechanism. The energy levels located below and closed to the Fermi level (determined by the calculated partial PDOS plots, Supporting Information Figures S1and S2) are ascribed to the energy levels of V_O and O_i centers, as shown in Figure 6d and e, respectively.[17k,n] It can be seen clearly that, at G, *Z* axis, the level location of V_O center is lower than that of O_i center. This indicates that the wavelength of visible emission arising from V_O center is shorter than that from O_i center, which is in agreement with the results of spectral analysis and the proposed luminescent mechanisms of visible emission for ZnO and ZnO:Zn powders. It should be noted that the calculated band gaps in semiconductors may be underestimated using this first-principles energy band calculation, probably due to many factors such as the action of the crystal field, the structure model, the defect density, the limits of method itself, and so forth.[17c,d] These factors are expected to give some contributions to the change of the calculated energy level, but were not included in view of the difficulty of doing so correctly. Nevertheless, the results of calculation can well explain the luminescence phenomenon and the proposed mechanism.

Effect of Annealing Temperatures on the Luminescence Intensities of ZnO Powders. To examine the effect of annealing temperatures on the luminescent intensities of ZnO powders, the as-prepared samples were annealed at various temperatures

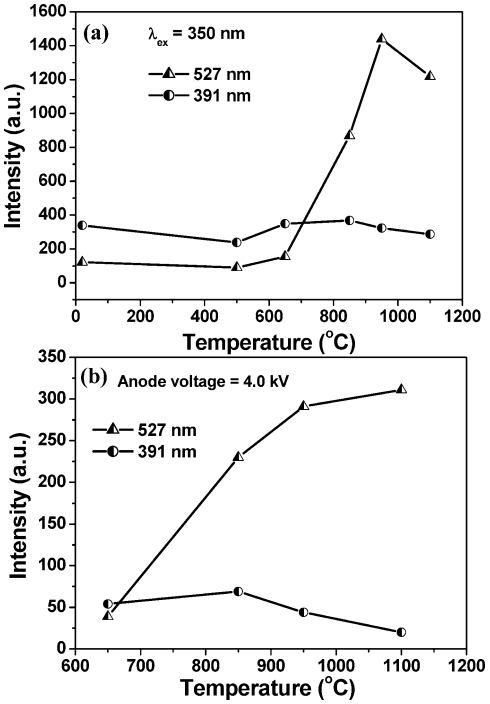

Figure 7. Effect of annealing temperatures on the PL (a) and CL (b) intensities of ZnO powders at the wavelength of 391 nm (circle) and 527 nm (triangle).

in air for 2h. Figure 7 shows the effect of annealing temperatures on the PL (a) and CL (b) intensities of ZnO powders at the wavelength of 391 nm (circle) and 527 nm (triangle). Excited with 350 nm UV light, the intensity of the visible emission at 527 nm is found to increase with increasing of annealing temperatures, reaching a maximum value after annealing at 950 °C, and then decreases. However, the intensity of the UV emission peaking near 391 nm is not affected strongly by the annealing temperature, as shown in Figure 7a. The changing trend of the CL intensities in the UV region is similar to that of the PL intensity, whereas in visible region, the CL intensity increases with raising of annealing temperatures, and above 950 °C, the increase is slow, as shown in Figure 7b. The as-prepared ZnO powders may possess a little of amorphous phases with a large number of structural defects and have residual organic solvent. This structural defects and residual solvent can act as nonradiative recombination centers, hence the intensities of the as-prepared ZnO powders in the visible region are relatively low. It is well-known that the annealing process can cause recovery of structural defects and form the accurate composition in ZnO powders, which can eliminate the nonradiative recombination centers efficiently.[3b] Thus, the emission intensity is improved significantly with increasing annealing temperatures. However, the single negatively charged interstitial oxygen ion (O_i^-) can be formed easily during the annealing process in air.[13c,14] The following reaction may occur at high temperatures:

$$ZnO \rightarrow ZnO_{1-x}\cdot x V_O^{\bullet}\cdot x O_i^- \quad (1)$$

At the same time, parts of the single ionized oxygen vacancies ($V_O^{\bullet}$) can be repaired by the O_2 that exists in air. The reaction may occur as follows:

$$ZnO_{1-x}\cdot x V_O^{\bullet}\cdot x O_i^- + {}^{y}/_{2}\, O_2 \rightarrow ZnO_{1-x+y}\cdot (x-y) V_O^{\bullet}\cdot x O_i^- - y e^- \quad (2)$$

The concentration of O_i^- increases with increasing of the annealing temperatures, which also leads to the enhancement of the PL and CL intensities.

In polycrystalline materials and in powders, band bending can occur at grain boundaries and then will create an electron depletion layer of width W at the particle surfaces.[3a] The electron depletion layer plays an important role in the green luminescence behavior of ZnO powders.[12a] In the electron depletion region, all oxygen vacancies are in the diamagnetic $V_O^{\bullet\bullet}$ state under flatband conditions.[11a] The intensity of the luminescence is influenced by the width of the depletion layer, which is also strongly dependent on defect density.[11c] The width of a depletion layer is given by[3a]

$$W = \left(\frac{2\epsilon_{ZnO} V_{bi}}{e N_D}\right)^{1/2}$$

where V_{bi} is the potential at the boundary, e is the electronic charge, N_D is the donor density, and ϵ_{ZnO} is the static dielectric constant of ZnO. From this formula, it can be seen that the width of the depletion layer is inversely proportional to the square root of the donor density. This dependence of the width of the depletion layer on donor density can be used to understand the variations of PL and CL intensities of ZnO powders observed in Figure 7. When the annealing temperature increases to 950 °C, the concentration of O_i^- will be saturated and not increase with the increasing of temperatures, so the PL intensity reaches the maximum value at this temperature. When the annealing temperatures are higher than 950 °C, the velocity of reaction 2 may be more quickly than that at lower temperatures, and the donor density in the powders may decrease, thus the width of the depletion layer will become larger. For a certain penetration depth of the photons beam, the visible emission originates from the bulk of the material,[11c] so the larger width of the depletion layer will lead to the decrease of luminescent centers being excited, thus resulting in the lower intensity. However, as for cathodoluminescence, the irradiation source is high energy electron beam, which possess higher penetration depth compared with photon beam, so the CL intensities increase slowly rather than decrease at the temperatures above 950 °C.

Effect of Reducing Temperatures on the Luminescence Intensities of ZnO:Zn Powders. To investigate the effect of the reducing temperatures on the PL and CL properties of ZnO:Zn powders, portions of ZnO-950 °C powders were reduced at different temperatures for 30 min. Figure 8 shows the PL (a) and CL (b) spectra of ZnO:Zn powders reduced at different temperatures. It is clearly observed that there are a sharp peak (∼390 nm) in the ultraviolet region and a broad emission band (yellow, ∼530 nm) in the visible region in the PL and CL spectra of ZnO:Zn powders reduced at 500 °C. With the increase of reducing temperatures, the PL intensities in visible region decreased first, reached minimum value at 800 °C (the visible emission disappeared completely), then a new broad emission band (green, ∼500 nm) appeared and its intensity increases with increasing of the reducing temperatures. The slight shifts of yellow emission or green emission with changing of reducing temperatures may be induced by the location change of interstitial oxygen ion (O_i^-) or the single ionized oxygen vacancy ($V_O^{\bullet}$) centers, and the location change may arise from the change in the local environments of the defect centers in different samples.[3a,11a] At the same time, the intensity of UV emission peaking near 390 nm increases first, reaching the maximum value at 800 °C, and then decreases. The variation of the CL spectra is similar to that of PL spectra, except that

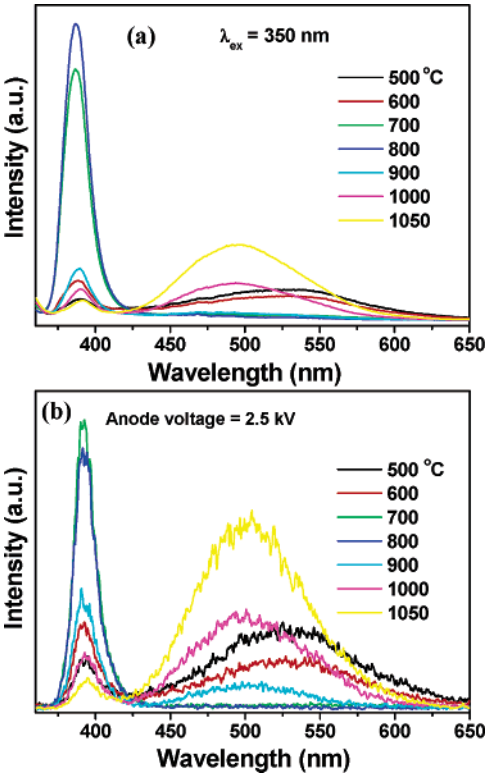

Figure 8. PL (a) and CL (b) spectra of ZnO:Zn powders reduced at different temperatures.

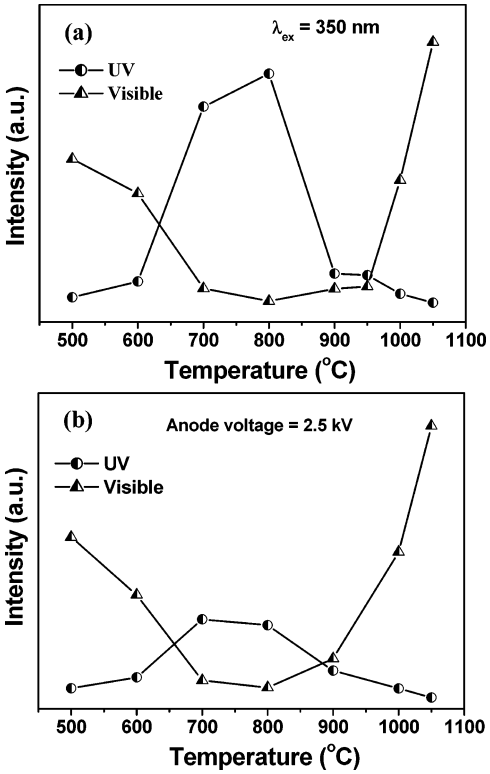

Figure 9. Effect of reducing temperatures on the PL (a) and CL (b) integral intensities of UV (circle) and visible (triangle) emission bands of ZnO:Zn powders.

the visible emission band disappeared and the UV emission intensity reached the maximum value at 700 °C, which may be due to the different excitation source. The two emission processes (i.e., visible emission band and exciton emission band) are in competition with each other, and the number of oxygen deficiency or other defects can be varied, which is then related to changes in the luminescence intensity.[11a,c] The cation-rich structure (anion vacancies) on the surface of a crystallite as emission centers can attract photogenerated electrons from the conduction band of ZnO particles.[18a] The variations of PL and CL intensities with the reducing temperatures can be seen directly from Figure 9, which is the effect of reducing temperatures on the PL (a) and CL (b) integral intensities of UV (circle) and visible (triangle) emission bands of ZnO:Zn powders.

As mentioned above, the broad emission band (centered at ~530 nm) of ZnO-950 °C powders arises from the single negatively charged interstitial oxygen ion (O_i^-) centers. Under the reducing treatment, the following reactions may occur:

$$ZnO_{1-x}\cdot xV_O^{\bullet}\cdot xO_i^- + xH_2 \rightarrow (1-x)ZnO\cdot xV_O^{\bullet} + xH_2O + xZn^0 + xe^- \quad (3)$$

$$ZnO + xH_2 \rightarrow ZnO_{1-x}\cdot xV_O^{\bullet} + xH_2O + xe^- \quad (4)$$

$$ZnO_{1-x}\cdot xV_O^{\bullet} + xe^- \rightarrow (1-x)\,ZnO + xZn_i^{2+} + 2xe^- \quad (5)$$

$$xZn_i^{2+} + 2xe^- \rightarrow xZn_i^0 \quad (6)$$

$$ZnO_{1-x}\cdot xV_O^{\bullet} + xZn^0 \rightarrow ZnO_{1-x}:xZn_O^0 + xe^- \quad (7)$$

$$xZn_i^0 \rightarrow xZn(g) \quad (8)$$

where Zn_i^0 is the interstitial zinc atom, and Zn_O^0 is the zinc atom occupied the oxygen vacancy. When the ZnO powders were reduced at low temperatures (e.g., 500 °C), though the density of O_i^- will decrease slightly due to the occurrence of the reaction 3, it is still high enough to arise the yellow emission in the visible region. With the increasing of reducing temperatures, the density of O_i^- decreases below the value that can lead to the yellow emission at 800 °C, while the density of $V_O^{\bullet}$ increases (reaction 4) and is still less than the value that can arise the green emission. We name the density of defect that can exactly cause the visible emission as the "critical density of defect luminescence" (CDDL). At 800 °C, both the density of O_i^- and $V_O^{\bullet}$ are below their CDDL, so no visible emission can be detected. When the reducing temperature is above 800 °C, the density of $V_O^{\bullet}$ will be higher than its CDDL and increase with the increasing of reducing temperatures, though there are some reactions (reactions 5, 7, etc.) that consume the $V_O^{\bullet}$. Because of the strong correlation between the green emission and the density of $V_O^{\bullet}$,[3a,12a] the intensities of green emission increase with increasing of reducing temperatures.

The increasing of the density of $V_O^{\bullet}$ can be confirmed by the EPR spectra. Figure 10 shows the EPR spectra of ZnO-950 °C (a), ZnO:Zn-800 °C (b), and ZnO:Zn-1050 °C (c) powders, respectively. There is only one EPR signal at $g = 1.9543$ in these three samples, which is due to the singly ionized oxygen vacancy ($V_O^{\bullet}$).[3a,12a,18b] The intensity of the EPR signal of ZnO-950 °C powders is the lowest, after the reducing treatment, the intensities of the signal increase with the increasing of the reducing temperatures. This indicates that the singly ionized oxygen vacancy exists in the ZnO and ZnO:Zn powders and its densities increase in the sequence of ZnO-950 °C < ZnO:Zn-800 °C < ZnO:Zn-1050 °C.[19] Though there is $V_O^{\bullet}$ defect in the ZnO-950 °C powders, the yellow emission may not arise from this defect because if $V_O^{\bullet}$ can lead to yellow emission,

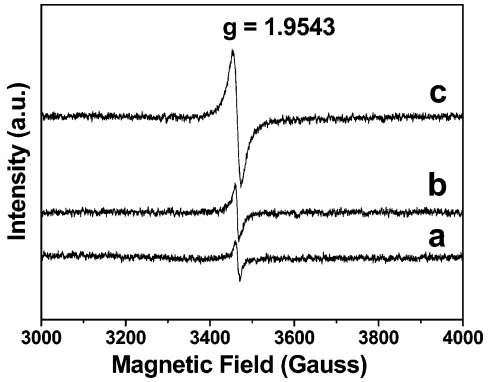

Figure 10. EPR spectra of ZnO-950 °C (a), ZnO:Zn-800 °C (b), and ZnO:Zn-1050 °C (c) powders. EPR spectra have been vertically shifted for clarity.

then the sample reduced at 800 °C should exhibit stronger yellow emission because of the higher density of $V_O^{\bullet}$ compared with that of the ZnO-950 °C powders. In fact, no visible emission can be observed for the ZnO:Zn-800 °C sample. This confirms the previous analysis; that is, there exists a critical density for defect luminescence: below the critical density, the defect center cannot lead to the visible emission. However, the UV emission may be affected strongly by the defects when its densities are near their critical density, as seen from Figure 9. In Figure 9a and b, when the reducing temperatures are in the range of 600−900 °C, the density of O_i^- decreased and then was below its CDDL at 800 °C, causing the yellow emission to decrease gradually and disappear completely, whereas the density of $V_O^{\bullet}$ increased, approaching to its CDDL at 800 °C and then exceeded, which leads to the appearance of green emission. At the same time, the intensities of UV emission increased remarkably, reaching the maximum value at 800 °C (for CL spectra at 700 °C), and then decreased evidently. Below 600 °C or above 900 °C, the intensities of UV emission varied indistinctively with the reducing temperatures. This indicates that the densities of O_i^- and $V_O^{\bullet}$ near their respective CDDL have a remarkable influence on the UV emission intensity. The effect of O_i^- and $V_O^{\bullet}$ defects on visible emissions is "counteracted" or "on balance" at about 800 °C so that ZnO:Zn-800 °C powders appear to be composed of rather pure defect-free ZnO crystallites.[5b] Above 900 °C, the intensities of green emission increased distinctively with increasing of reducing temperatures, which resulted from the increasing of $V_O^{\bullet}$ density and the thinner of the width of the depletion layer.[11a]

Effect of Filament Current and Accelerating Voltage on the CL Spectra. The CL intensities of ZnO:Zn-1050 °C powders as a function of filament current (a) and accelerating voltage (b) are shown in Figure 11. From Figure 11a it can be seen that the CL intensities increase with increasing the filament current from 89.2 to 102.8 mA under the fixed anode voltage of 0.8 kV. When the filament current is fixed at 96.0 mA, the CL intensities increase with increasing the anode voltage from 0.8 to 3.0 kV, as shown in Figure 11b. It is known that the penetration depth of beam electrons into a particular specimen is determined by the energy of the beam electrons. The higher the energy, the greater the penetration depth. The electron penetration depth (L) can be estimated by the empirical formula: $L[\text{Å}] = 250(A/\rho)(E/Z^{1/2})^n$, where $n = 1.2/(1-0.29\log_{10}Z)$, and A is the atomic or molecular weight of the material, ρ is the density, Z is the atomic number or the number of electrons per molecule in the case compounds, and E is the anode voltage (kV).[20] For ZnO phosphors, the electron penetration depth at the accelerating voltage of 1−3 kV is estimated to be 7−74 nm. For cathodoluminescence, the luminescent centers are excited by the plamons produced by the incident electrons. Hence, with the increase of the anode voltage, more plasmons will be produced by the incident electrons, resulting in more luminescent centers being excited and thus higher CL intensity.[21]

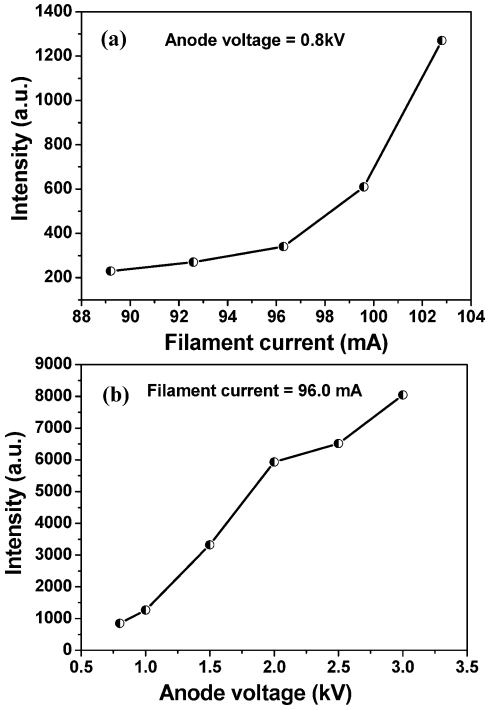

Figure 11. CL intensities of ZnO:Zn-1050 °C powders as a function of filament current (a) and anode voltage (b).

4. Conclusions

Microcrystalline ZnO and ZnO:Zn powder phosphors have been prepared by the polyol-method followed by annealing in air and reducing gas, respectively. The obtained ZnO and ZnO:Zn powders possess the hexagonal structure with the particle size in the range of 1−2 μm. The ultraviolet, yellow, and green emissions of ZnO powders can be tuned by altering the annealing conditions. The PL and CL spectra of ZnO powders annealed at 950 °C in air have a broad and strong emission band centered at about 527 nm (yellow). When the ZnO-950 °C sample was reduced at 800 °C, the yellow emission disappeared completely, while the ultraviolet emission band became the strongest. Reduced above this temperature, the green emissiom (∼500 nm) appeared and increased with the increasing of reducing temperatures. The yellow and green emissions may be attributed to the transitions of photogenerated electron close to the conduction band to the deeply trapped hole in the O_i^- and $V_O^{\bullet}$ centers, respectively.

Acknowledgment. This project is financially supported by the foundation of "Bairen Jihua"of Chinese Academy of Sciences, the MOST of China (no. 2003CB314707), and the National Natural Science Foundation of China (50225205, 50572103, and 20431030). We are indebted to Prof. Siyuan Zhang for useful suggestions.

Supporting Information Available: The molar ratios of Zn to O atom ($R_{Zn/O}$) and the calculated DOS of ZnO. This material is available free of charge via the Internet at http://pubs.acs.org.

References and Notes

(1) (a) Holloway, P. H.; Trottier, T. A.; Abrams, B.; Kondoleon, C.; Jones, S. L.; Sebastian, J. S.; Thomes, W. J.; Swart, H. *J. Vac. Sci. Technol., B* **1999**, *17*, 758. (b) Jüstel, T.; Nikol, H.; Ronda, C. *Angew. Chem., Int. Ed.* **1998**, *37*, 3084.

(2) Yamamoto, H.; Isogai, H.; Yoshida, Y. *Thin Solid Films* **2001**, *383*, 89.

(3) (a) Vanheusden, K.; Warren, W. L.; Seager, C. H.; Tallant, D. R.; Voigt, J. A.; Gnade, B. E. *J. Appl. Phys.* **1996**, *79*, 7983. (b) Li, W.; Mao, D. S.; Zhang, F. M.; Wang, X.; Liu, X. H.; Zou, S. C.; Zhu, Y. K.; Li, Q.; Xu, J. F. *J. Vac. Sci. Technol., A* **2000**, *18*, 2295. (c) Ozawa, L.; Itoh, M. *Chem. Rev.* **2003**, *103*, 3835.

(4) (a) Mordkovich, V. Z.; Hayashi, H.; Haemori, M.; Fukumura, T.; Kawasaki, M. *Adv. Funct. Mater.* **2003**, *13*, 519. (b) Vecht, A.; Smith, D. W.; Chadha, S. S.; Gibbons, C. S.; Koh, J.; Morton, D. *J. Vac. Sci. Technol., B* **1994**, *12*, 781.

(5) (a) Ogata, K.; Sakurai, K.; Fujita, Sz.; Fujita, Sg.; Matsushige, K.; *J. Cryst. Growth* **2000**, *214/215*, 312. (b) Cho, S.; Ma, J.; Kim, Y.; Sun, Y.; Wong, G. K. L.; Ketterson, J. B. *Appl. Phys. Lett.* **1999**, *75*, 2761.

(6) (a) Wei, J.; Zhang, B.; Yao, N.; Wang, X.; Ma, H.; Wang, S. *J. Vac. Sci. Technol., B* **2001**, *19*, 1082.

(7) (a) Lee, Y. H.; Song, M. H.; Ju, B. K.; Shin, D. K.; Oh, M. H. *J. Vac. Sci. Technol., B* **1997**, *15*, 512. (b) Bylander, E. G. *J. Appl. Phys.* **1978**, *49*, 1188. (c) Leskelä, M. *J. Alloys Compd.* **1998**, *275*−*277*, 702. (d) Pennebaker, W. B.; O'Hanlon, J. F. *J. Appl. Phys.* **1974**, *45*, 1315.

(8) (a) Lin, C. H.; Chiou, B.-S.; Lin, J. D. *J. Mater. Sci.* **2002**, *13*, 705. (b) Lin, L. H.; Chiou, B.-S.; Chang, C. H.; Lin, J. D. *Mater. Chem. Phys.* **2002**, *77*, 647. (c) Lin, C. H.; Chiou, B.-S.; Chang, C. H.; Lin, J. D. *J. Mater. Sci.* 2002, *13*, 1.

(9) Hunt, C. E.; Chakhovskoi, A. G. *J. Vac. Sci. Technol., B* **1997**, *15*, 516.

(10) (a) Li, W.; Mao, D.; Zhang, F.; Wang, X.; Liu, X.; Zou, S.; Zhu, Y.; Li, Q.; Xu, J. *J. Vac. Sci. Technol., B* **2001**, *19*, 1004. (b) Nakanishi, Y.; Miyake, A.; Kominami, H.; Aoki, T.; Hatanaka, Y.; Shimaoka, G. *Appl. Surf. Sci.* **1999**, *142*, 233. (c) Seelig, E. W.; Tang, B.; Yamilov, A.; Cao, H.; Chang, R. P. H. *Mater. Chem. Phys.* **2003**, *80*, 257.

(11) (a) Wu, X. L.; Siu, G. G.; Fu, C. L.; Ong, H. C. *Appl. Phys. Lett.* **2001**, *78*, 2285. (b) van Dijken, A.; Meulenkamp, E. A.; Vanmaekelbergh, D.; Meijerink, A. *J. Lumin.* **2000**, *90*, 123. (c) van Dijken, A.; Meulenkamp, E. A.; Vanmaekelbergh, D.; Meijerink, A. *J. Phys. Chem. B* **2000**, *104*, 1715. (d) Bahnemann, D. W.; Kormann, C.; Hoffmann, M. R. *J. Phys. Chem.* **1987**, *91*, 3789.

(12) (a) Vanheusden, K.; Seager, C. H.; Warren, W. L.; Tallant, D. R.; Voigt, J. A. *Appl. Phys. Lett.* **1996**, *68*, 403. (b) Kröger, F. A.; Vink, H. J. *J. Chem. Phys.* **1954**, *22*, 250. (c) Mahan, G. D. *J. Appl. Phys.* **1983**, *54*, 3825.

(13) (a) Liu, M.; Kitai, A. H.; Mascher, P. *J. Lumin.* **1992**, *54*, 35. (b) Fujihara, S.; Ogawa, Y.; Kasai, A. *Chem. Mater.* **2004**, *16*, 2965. (c) Wen, F.; Li, W.; Moon, J.-H.; Kim, J. H. *Solid State Commun.* **2005**, *135*, 34.

(14) Lin, B.; Fu, Z.; Jia, Y. *Appl. Phys. Lett.* **2001**, *79*, 943.

(15) (a) Djurišić, A. B.; Leung, Y. H.; Choy, W. C. H.; Cheah, K. W.; Chan, W. K. *Appl. Phys. Lett.* **2004**, *84*, 2635. (b) Li, D.; Leung, Y. H.; Djurišić, A. B.; Liu, Z. T.; Xie, M. H.; Shi, S. L.; Xu, S. J.; Chan, W. K. *Appl. Phys. Lett.* **2004**, *85*, 1601. (c) Djurišić, A. B.; Choy, W. C. H.; Roy, V. A. L.; Leung, Y. H.; Kwong, C. Y.; Cheah, K. W.; Rao, T. K. G.; Chan, W. K.; Lui, H. F.; Surya, C. *Adv. Funct. Mater.* **2004**, *14*, 856.

(16) (a) Wei, H.; Wu, Y.; Wu, L.; Hu, C. *Mater. Lett.* **2005**, *59*, 271. (b) Zhou, Y. X-ray Photoelectron Spectroscopy. In *Technology of Materials Analysis and Characterization*; Zhou, Y., Wu, G., Eds.; Harbin Institute of Technology Publications: Harbin, 1998; p 229.

(17) (a) Segall, M. D.; Lindan, P. L. D.; Probert, M. J.; Pickard, C. J.; Hasnip, P. J.; Clark, S. J.; Payne, M. C. *J. Phys. Condens. Mater.* **2002**, *14*, 2717. (b) Perdew, J. P.; Ernzerhof, B. M. *Phys. Rev. Lett.* **1996**, *77*, 3865. (c) Fu, Z.; Zhou, S.; Zhang, S. *J. Solid State Chem.* **2005**, *178*, 230. (d) Fu, Z.; Zhou, S.; Yu, Y.; Zhang, S. *Chem. Phys. Lett.* **2004**, *395*, 285. (e) Gale, J. D.; Rohl, A. L.; Milman, V.; Warren, M. C. *J. Phys. Chem. B* **2001**, *105*, 10236. (f) Zhang, Y.; Cheng, W.; Wu, D.; Zhang, H.; Chen, D.; Gong, Y.; Kan, Z. *Chem. Mater.* **2004**, *16*, 4150. (g) Liu, X. J.; Wu, Z. J.; Hao, X. F.; Xiang, H. P.; Meng, J. *Chem. Phys. Lett.* **2005**, *416*, 7. (h) Xiang, H. P.; Wu, Z. J.; Meng, J. *Phys. Status Solidi B* **2005**, *242*, 1414. (i) Wang, Y. X.; Arai, M.; Sasaki, T.; Wang, C. L. *Phys. Rev. B* **2006**, *73*, 035411. (j) Kohan, A. F.; Ceder, G.; Morgan, D.; Van de Walle, C. G. *Phys. Rev. B* **2000**, *61*, 15019. (k) Erhart, P.; Klein, A.; Albe, K. *Phys. Rev. B* **2005**, *72*, 085213. (l) Lu, Y.; Zhong, J. Zinc Oxide-Based Nanostructures. In *Semiconductor Nanostructures for Optoelectronic Applications*; Steiner, T.; Ed.; Artech House, Inc., 2004; p 187. (m) Vanderbilt, D. *Phys. Rev. B* **1990**, *41*, 7892. (n) Lee, E.-C.; Kim, Y.-S.; Jin, Y.-G.; Chang K. J. *Phys. Rev. B* **2001**, *64*, 085120.

(18) (a) Koch, U.; Fojtik, A.; Weller, H.; Henglein, A. *Chem. Phys. Lett.* **1985**, *122*, 507. (b) Kasai, P. H. *Phys. Rev.* **1963**, *130*, 989.

(19) Vanheusden, K.; Seager, C. H.; Warren, W. L.; Tallant, D. R.; Caruso, J.; Hampden-Smith, M. J.; Kodas, T. T. *J. Lumin.* **1997**, *75*, 11.

(20) Feldman, C. *Phys. Rev.* **1960**, *117*, 455.

(21) Wang, H.; Lin, C. K.; Liu, X. M.; Lin, J.; Yu, M. *Appl. Phys. Lett.* **2005**, *87*, 181907−1.